Beyond Tafel Analysis for Electrochemical CO2 Reduction

Kaitlin Rae M. Corpus[1,2‡], Justin C. Bui[1,2‡], Aditya M. Limaye[3], Lalit M. Pant[4,5], Karthish Manthiram[6,7], Adam Z. Weber[2,4], & Alexis T. Bell[1,2*]

[1] Department of Chemical and Biomolecular Engineering
University of California Berkeley
Berkeley, CA 94720, USA

[2] Liquid Sunlight Alliance
Lawrence Berkeley National Laboratory
Berkeley, CA 94720, USA

[3] Department of Chemical Engineering
Massachusetts Institute of Technology
Cambridge, MA 02139, USA

[4] Energy Technologies Area
Lawrence Berkeley National Laboratory
Berkeley, CA 94720, USA

[5] Department of Sustainable Energy Engineering
Indian Institute of Technology, Kanpur
Kanpur, UP-208016, India

[6] Division of Chemistry and Chemical Engineering
California Institute of Technology
Pasadena, CA 91125, USA

[7] Liquid Sunlight Alliance
California Institute of Technology
Pasadena, CA 91125, USA

Corresponding Author: alexbell@berkeley.edu
Phone: (510)-642-1536
‡Contributed equally

1.   Abstract

The development and characterization of active and selective catalysts is critical for the simulation and optimization of electrochemical synthesis of chemicals and fuels using renewable energy. The rate of electrochemical generation of a specific product as a function of electrode potential can be described by a Tafel equation, which depends on two parameters: the Tafel slope (or the related transfer coefficient) and the exchange current density. However, common methods for calculating Tafel slopes are subjective and limited by data insufficiency resulting from challenges associated with product quantification, and, as shown here, the effects of mass transport, bulk reaction occurring in the mass-transfer boundary layer, and the occurrence of competitive surface reactions. Errors in the Tafel slope extracted from experimental data can also lead to errors in the exchange current density estimation. To address these issues, we present a technique that leverages statistical learning methods informed by physics-based modeling to calculate kinetic parameters (the transfer coefficient and exchange current density) with quantified uncertainty. The method is applied to 21 sets of data for the electrochemical reduction of CO_2 to CO and H_2 on Ag catalysts acquired under similar experimental conditions. We find that fitted values for the transfer coefficient and exchange current density do not converge to a unique set of values, and that there is an apparent correlation of these parameters; however, the most probable value of the exchange coefficient for CO and H_2 formation correspond reasonably well with the DFT-predicted values of this parameter. While the system explored is relatively simple, the techniques developed can be used to evaluate the transfer coefficient and exchange current density for many other electrochemical processes.

2.   Introduction

Electrochemical reduction of CO_2 emitted from point sources (e.g., cement production, separation from natural gas, iron and aluminum ore smelting, and fermentation of sugars) using electricity from renewable resources (e.g., wind and solar) offers a means for recapturing its carbon content. Moreover, if the CO_2 can be taken from the atmosphere and converted electrochemically to chemicals and fuels, one could envision a closed carbon cycle.[1–4] In order to produce desired products with high rates and selectivity, it is important to understand how to design electrochemical cells that enable achievement of these objectives.[5–8] A key element in pursuit of this goal is accurate representation of the rates individual product formation rates and their dependence on reactant concentration, pH, and cathode potential.

For the design and simulation of electrochemical processes, the current density (i_j) for producing product j is most commonly based on the Butler-Volmer equation (Equation (1)) or the simpler Tafel equation (Equation (2)), which is based on the assumption that the reaction is irreversible at large overpotentials. In this work we only consider the Tafel equation for the cathodic direction.

$$i_j = i_{0,j}\left(-\exp\left(-\frac{\alpha_{c,j}F}{RT}\eta_j\right) + \exp\left(\frac{\alpha_{a,j}F}{RT}\eta_j\right)\right) \tag{1}$$

$$i_j = -i_{0,j}\,exp\left(-\frac{\alpha_{c,j}F}{RT}\eta_j\right) \tag{2}$$

Here R is the ideal gas constant, F is Faraday's constant, η_j is the overpotential or driving force for the electrochemical reaction j, T is the absolute temperature, $\alpha_{c,j}$ is the transfer coefficient, and $i_{0,j}$ is the exchange current density. In Equation (2) there are two important parameters, the

transfer coefficient ($\alpha_{c,j}$) that describes the sensitivity of the product current density to changes in the overpotential (*i.e.,* the electrochemical driving force) and the exchange current density ($i_{0,j}$), the pre-factor for the exponential term.[9] It is important to note that the exchange current density contains explicit concentration dependences on the reactants and products of a given reaction, as discussed in Section **S3** of the **SI**. Many studies of electrochemical synthesis report the Tafel slope, which is directly related to the transfer coefficient defined as the overpotential required to obtain a ten-fold increase in product current density.[9,10]

$$\text{Tafel Slope} = -\frac{\log(10)\,RT}{\alpha_{c,j}F} = \frac{59.125\,[\text{mV dec}^{-1}]}{\alpha_{c,j}} \text{ for } T = 298\text{ K} \tag{3}$$

For multi-step kinetics, the Tafel slope, or related the transfer coefficient $\alpha_{c,j}$, has been used to infer which elementary step is rate-limiting in the formation of a particular reaction product.[11–13]

A commonly used method to calculate Tafel slopes involves a least-squares regression on the linear portion of the logarithm of the measured current density vs cathode voltage (i.e., the kinetic region) excluding data that lie in the mass-transport limited regime (**Figure 1**, **top**).[10] For the electrochemical reduction of CO_2, the mass-transport-limited regime occurs at potentials for which the predicted rate of CO_2 consumption by electrochemical and homogeneous chemical reactions becomes greater than the rate of CO_2 transport to the surface. Mass-transport limitations in CO_2R are caused primarily by the low solubility and diffusion coefficient of CO_2 in the aqueous electrolyte.[14,15] Because the regimes of kinetic control and the onset of mass-transfer control are defined arbitrarily, this method of identifying the regime of kinetic control is prone to human error and leads to a reduction in the number of data points available for analysis. It is also notable

that in electrochemical synthesis the product must be quantified at every applied potential through time-consuming steady-state measurements. The need for product quantification contrasts with water electrolysis for which catalytic behavior can be measured rapidly at thousands of points via linear-sweep voltammetry. Because data in electrochemical synthesis must be collected by steady-state chronopotentiometry or chronoamperometry to generate sufficient product for quantification, rapid current-voltage sweeps are impractical if one wants to determine the partial current densities for each product. In other words, the steady-state nature of electrochemical synthesis, in which multiple products are formed, limits the number of available data points for each product.
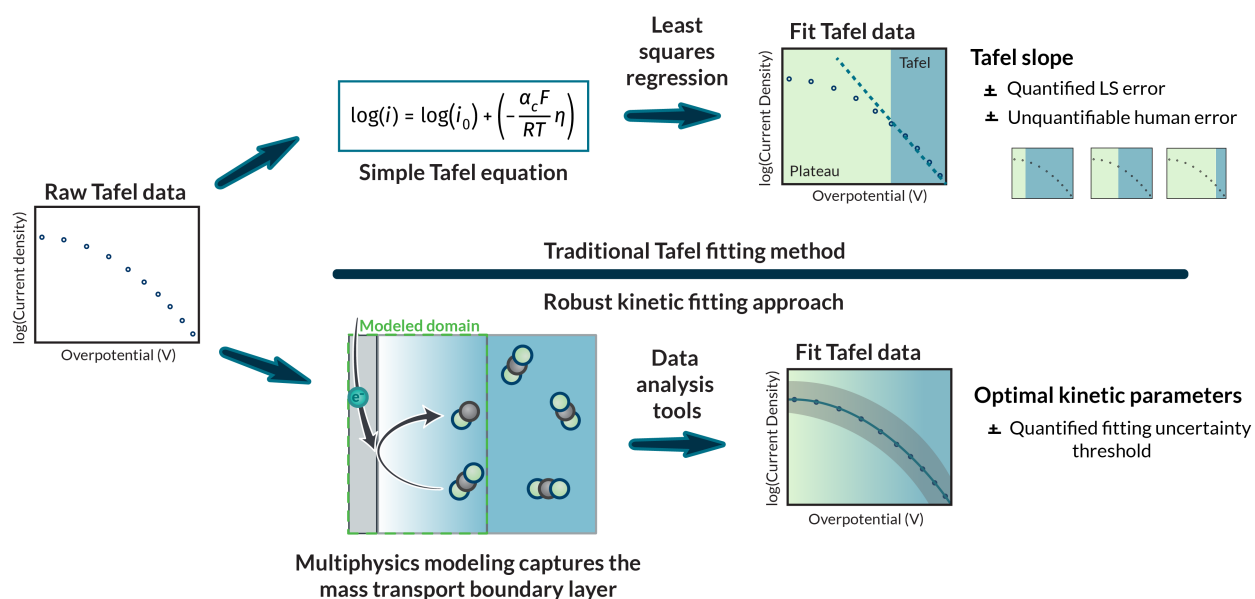

Figure 1: Schematic of **(top)** traditional method of processing electrochemical data via Tafel analysis and its associated, unquantifiable human error, and **(bottom)** proposed robust kinetic fitting approach which uses detailed physical models inform data analysis tools to obtain kinetic parameters with quantifiable uncertainty.

Prior work has sought to address these concerns and provide rigorous methods for determining kinetic parameters.[10,16,17] Recently, Limaye *et al.* have attempted to address the

challenge of data insufficiency in Tafel analysis for electrochemical CO_2 reduction by using a Bayesian learning algorithm,[10] in which current-voltage data are fit to a representation of the intrinsic reaction rate given by the Tafel equation together with the effects of mass transfer. Using such a model enabled fitting of all experimental data without the need to arbitrarily define the Tafel region, even for limited data sets (5-20 data points). Furthermore, the Bayesian learning model used in this work provided a distribution of potential Tafel slopes and a defined uncertainty threshold. This approach revealed the human errors in involved fitting Tafel slopes reported in the literature. A limitation of this work is that the physical model employed did not account for coupling of mass transfer effects with competing electrochemical and homogeneous buffer reactions that consume reactants and change local pH,[18–20] as well as the complex dependences of the intrinsic kinetics on species activities that affect observed kinetics.[7,19,21,22]

In this work, we present a one-dimensional, reaction-transport model of the electrochemical reduction of CO_2 to CO and H_2 over an Ag catalyst that is then used in combination with advanced data-analysis tools to fit the Tafel parameters (i.e., α_c and i_0) for a variety of Ag catalysts. This approach provides a rigorous means for identifying the parameters required for continuum simulations. Application of this approach to 21 data sets for CO_2 reduction to CO on Ag in similar experimental setups reveals that the fitted rate parameters are broadly distributed, probably due to differences in catalyst morphology (*i.e.*, distribution of surface facets and roughness). The methodology reported here provides a rigorous approach for determining the Tafel parameters associated with product partial current densities vs cathodic potential curves obtained for electrochemical processes that produce multiple products. This

finding is particularly important for systems in which the formation of one product influences the rate of formation of other products through the effects of mass transfer and bulk reactions.

3.   Methods

3.1. Continuum Model

Figure 2 illustrates the one-dimensional (1-D) model used to simulate mass transport and reaction occurring in an electrochemical cell performing CO_2 reduction. The modeled domain consists of a planar Ag electrode, an aqueous potassium bicarbonate ($KHCO_3$) electrolyte, and the associated mass-transport boundary layer. The bulk concentration of the $KHCO_3$ electrolyte is chosen to coincide with that used in the experimental data set to be fitted, and the thickness of the associated mass-transport boundary layer (L_{BL}) is fit along with the kinetic parameters. We note further that all of the experimental data examined in this study were acquired using a flow cell (*i.e.,* an H-cell) with well-defined hydrodynamics and a reference electrode located in the potassium bicarbonate electrolyte (**Figure 2a**).[23–33] The decision to consider only Ag catalysts used under similar experimental conditions limits the amount of available data in literature, but enables deconvolution of the catalytic behavior from other variables. We note that previous work has shown that a 1-D representation is capable of capturing the requisite concentration and potential gradients needed to model aqueous CO_2 reduction on planar catalysts.[14,34,35]
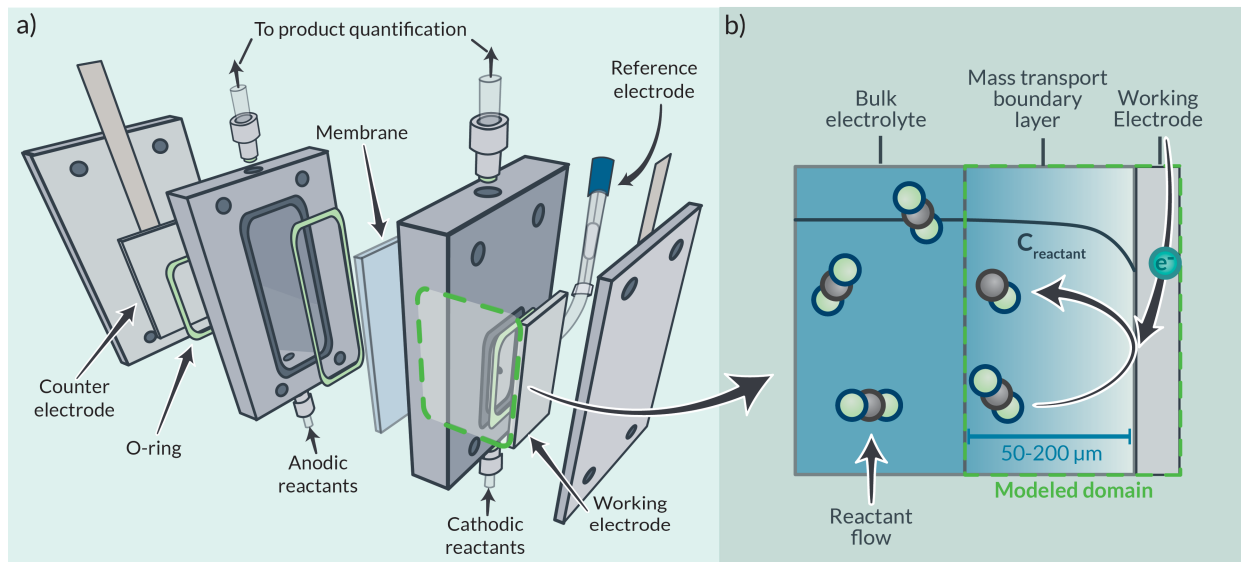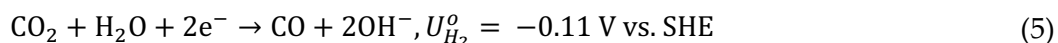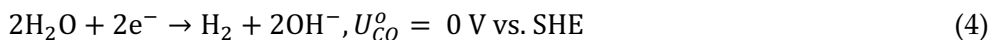
Figure 2: Schematic representation **(a)** a typical experimental set up, and **(b)** the corresponding modeled domain for the boundary layer model.

The CO and H_2 evolution reactions (COER and HER) occur at the surface of the Ag electrode, with the following stoichiometries and standard potentials.

$$2H_2O + 2e^- \rightarrow H_2 + 2OH^-, U_{CO}^o = 0 \text{ V vs. SHE} \tag{4}$$

$$CO_2 + H_2O + 2e^- \rightarrow CO + 2OH^-, U_{H_2}^o = -0.11 \text{ V vs. SHE} \tag{5}$$

A concentration-dependent Tafel expression was used for each product to model the kinetics of the competing reactions (for which the kinetic parameters will be fit),

$$i_{CO} = \left(\frac{a_{CO_2}}{a_{CO_2}^{bulk}}\right)^{-\gamma_{CO_2,CO}} \left(\frac{a_{OH^-}}{a_{OH^-}^{bulk}}\right)^{\gamma_{OH^-,CO}} i_{0,CO}\left\{-\exp\left[-\frac{\alpha_{c,CO}F}{RT}\eta_{s,CO}\right]\right\} \tag{6}$$

$$i_{H_2} = \left(\frac{a_{OH^-}}{a_{OH^-}^{bulk}}\right)^{\gamma_{OH^-,H_2}} i_{0,H_2}\left\{-\exp\left[-\frac{\alpha_{c,H_2}F}{RT}\eta_{s,H_2}\right]\right\} \tag{7}$$

where $i_{0,j}$ and $\alpha_{c,j}$ are the exchange current density and cathodic transfer coefficient for product j, respectively. These parameters are obtained by our fitting method described in **Section 3.4**. $\gamma_{i,j}$ represents the rate order of species i in the reaction to form species j and is constrained by its relationships to the transfer coefficients, as given by **Equations S8-10**. Here, a_i represents the

activity of species i locally at the electrode surface, as calculated by the reaction-transport simulation, and a_i^{bulk} represents the activity of species i in the bulk electrolyte. The terms involving the ratio of the surface and bulk activity account for mass-transport and concentration gradients within the boundary layer. $\eta_{s,i}$ is the surface overpotential for a given electrochemical reaction defined in **Equations S15** and **S16** in the **SI**. A detailed description of the physics employed in the model, as well as a generalized derivation of the kinetic model, can be found in the **SI, Sections S1-3**.

3.3 Covariance Matrix Adaptation Evolution Strategy

To minimize the objective function, which in this case is the mean square error (MSE) of the fit to the CO and H₂ specific polarization curves, the covariance matrix adaptation evolutionary strategy (CMA-ES) was employed (shown schematically in **Figure 3**). CMA-ES is a global, derivative-free optimization method that operates by forming a parametric distribution over the solution space. It samples a population of solution candidates iteratively, typically from a multivariate gaussian distribution.[36] This objective function is then evaluated for each candidate set of parameters. After evaluating the objective function for each point in a given generation of solution candidates, the solutions are sorted by the magnitude of the objective function and the distribution parameters (the mean vector and covariance matrix) are updated based on the ranking of objective function values. The goal is to search for the optimum set of parameters, such that the objective function is a minimum. The method stops once the change in error across generations has dropped below a certain tolerance (in this study, a tolerance of 1×10^{-11} was used, which is the default in CMA-ES algorithm in MATLAB.) It is critical to note that CMA-ES

is gradient-free since the objective function used for fitting the Tafel kinetic is non-convex, so there exist many local minima in which a gradient-descent method can get trapped. Notably, previous work has shown that small changes in the fitted Tafel parameters can lead to local minima that approximately fit experimental data.[17] We also note (**Section S4.1** of the **SI**) that using a gradient-descent method (e.g., MATLAB's fmincon) in lieu of the CMA-ES method ultimately fails to fit experimental polarization data (**Section S10** of the **SI**).
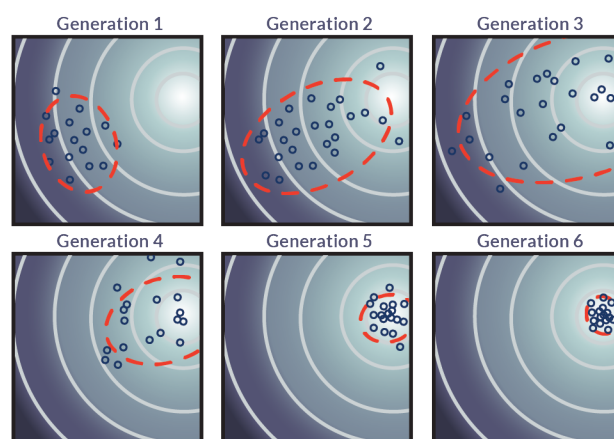

Figure 3: Schematic process of a typical evolution process in CMA-ES for a two-parameter optimization. In the first generation (Generation 1), the CMA-ES creates a generation of points with values of the parameters assigned by an initial Gaussian distribution with a mean at the center of given elliptical bounds and the radii of the ellipse determined by the standard deviations of the distribution (red-dashed lines). CMA-ES ranks the points in terms of how close they are to minimizing the objective function (white locus of the plots) and moves the distribution in the direction of the points with the best ranking regarding objective minimization. In the following generations, the (Generations 2-5) this process is repeated and continues. As the points move closer to the global minimum, the CMA-ES begins to shrink the standard deviation and converge upon the global minimum. The process stops (Generation 6) when the standard deviation of the points reaches a specified, small value, indicating that the generated points all converge upon the global minima.

3.3.1 Quantification of the Uncertainty in the Parameters Obtained from CMA-ES

To quantify the uncertainty in the parameters values obtained from CMA-ES, samples of the parameters were drawn from the last 25, 50, and 75% of solution candidates seeded by the

CMA-ES optimizer (all tested $L_{BL}, i_{0,H_2}, \alpha_{H_2}, i_{0,CO},$ and α_{CO}). The last 25% of points were representative of the final generations of CMA-ES, and the 50%- and 75%-point samples were representative of earlier generations that were further from but still close to convergence (due to the incredibly stringent tolerance of 1×10^{-11}). The uncertainties in the fitted parameters were defined by one standard deviation of the selected CMA-ES-generated parameter points (**Tables S9-11**). For each of these groupings (last 25, 50, and 75%), the current densities at all simulated applied potentials (*i.e.*, the polarization curves) were evaluated for each of the parameter groupings, and the standard deviation of the current density was calculated at every simulated potential to define the uncertainty band for the fitted polarization curves. Because of the stringent convergence criteria employed, there was very little change in the objective function for the last 25% of evaluated candidates, meaning that the uncertainty for the last 25% of candidate points was exceedingly small.

3.4 Description of Fitting Method

The process shown schematically in **Figure 4** was used to fit the experimental data. First, the reported cathode potentials (usually referenced to a reversible hydrogen electrode (RHE)) were shifted to the standard hydrogen electrode (SHE) potential, by (see **Figure 4B**):

$$\phi_c[\text{V vs. SHE}] = \phi_c[\text{V vs. RHE}] - 0.059 \times \text{pH}_{\text{bulk}} \tag{8}$$

This change of reference makes the experimentally measured potentials consistent with the potentials used in the model (**Section S1-3** of the SI).
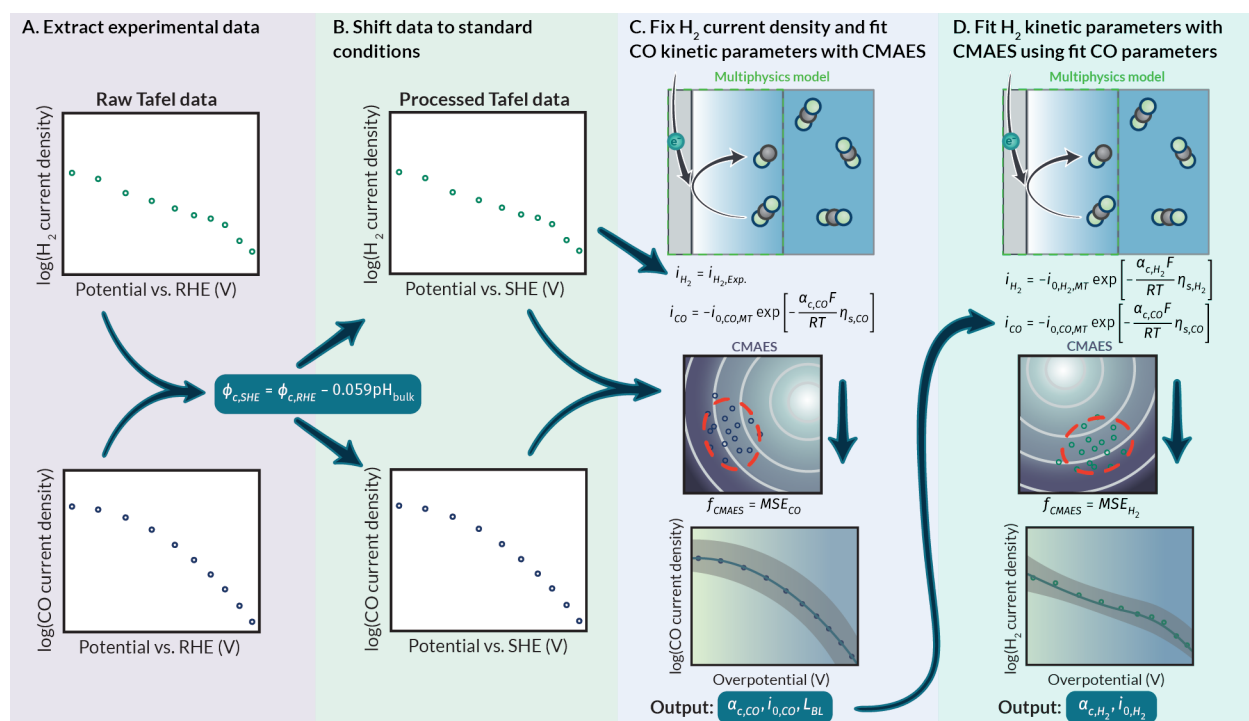
Figure 4: Process diagram depicting the inputs, outputs, and steps taken to extract kinetic parameters from a given set of experiments using the developed method. **(A)** Extraction of experimental Tafel data. **(B)** Shifting of Tafel data to standard conditions. **(C)** (Top to bottom) Fixing of H_2 current density in COMSOL simulation, fitting CO kinetic parameters with CMA-ES, and quantifying uncertainty. **(D)** (Top to bottom) Using fit CO kinetics from **(C)** in the COMSOL model and running CMA-ES to fit H_2 kinetic parameters and extract uncertainty. In panels **(C)** and **(D)**, $i_{0,k,MT}$ represents the product of the traditional $i_{0,k}$ and the mass-transport activity terms in the Tafel expression shown in Equations (6) and (7).

Next, the parameters for each reaction were fitted one reaction at a time in order to separate the $((2k \times 2k) + 1)$ dimensional optimization problem (where k is the number of competing reactions and the $+ 1$ is due to fitting L_{BL}) into $(k - 1)$ 2-dimensional optimizations and a single 3-dimensional optimization (in which the thickness of the boundary layer is fit). This procedure makes the problem more tractable and avoids the so-called "curse of dimensionality" in optimizations.[36] It is also important to note that fitting the boundary layer was necessary to provide the best fit for the CO data, as the boundary-layer thickness dictates the mass-transport-limiting plateau (see **Figure S1**), and is seldom measured or reported for CO_2R current densities

measured using a flow cell. We note that the fitted mass-transport boundary-layer thicknesses generally agree in terms of order of magnitude with values reported in previous flow cell studies; any discrepancies are likely due to assumed Sherwood relationships for the calculation of the mass-transfer coefficient, which, in most cases, do not account for the effects of homogeneous buffer reactions and multi-ion transport.[15]

To fit the kinetics for CO formation, the reference-shifted experimental data for H_2 partial current density versus voltage are imported into the CMA-ES algorithm and are held fixed. Doing so is critical for calculating the kinetic parameters for CO formation because H_2 data enable the model to calculate changes in the local pH and CO_2 concentration that result from HER, which, in turn, affect kinetics of CO formation. The COER current density is defined by Equation (6). The CMA-ES algorithm then uses the transport and reaction model to obtain the best values of $\alpha_{c,CO}$, $i_{0,CO}$, and L_{BL} that give the best fit to the data (**Figure 4C**). Once the CO kinetic parameters and L_{BL} are determined, they are fixed to their fitted values and the parameter for the HER partial current, α_{H_2} and i_{0,H_2}, described by Equation (7) are fitted using the CMA-ES algorithm (**Figure 4D**). Post processing of the CMA-ES distributions provides the uncertainty. This process can be easily generalized to a system containing a greater number of competing reactions as described in Section **S4.2** of the **SI**. While this overall process could be repeated to further reduce error, doing so results in only a minor change in the fitted parameters ($< 0.1\%$ change in α, $< 0.2\%$ change in L_{BL}, and $< 0.7\%$ change in i_0) and comes at greater computational expense. Thus, for this work, the fitting process was run once through each product.

4.   Results and Discussion

4.1 Continuum Modeling to Assess Traditional Tafel Fitting

To assess the impact of mass transport and bulk reactions on observed partial current densities, a sensitivity analysis was carried out (**Section S5**). By this means, the sensitivity of the product partial current densities to changes in the kinetic parameters ($\alpha_{i,c}$ and $i_{i,0}$) is determined (**Figure S2-3**). This procedure enables an assessment of the degree of sensitivity between the outputs and input parameters in the model (*i.e.,* how much an output parameter changes when an input parameter is changed). When an output is positively sensitive to an input, an increase in the input results in an increase in the output; when an output is negatively sensitive to an input, an increase in the input results in a decrease in the output. The sensitivity analysis revealed that the CO partial current density is highly negatively sensitive to mass transfer (*i.e.,* L_{BL}) due to low availability of CO_2 in the aqueous electrolyte; however, the H_2 partial current density is less sensitive to mass-transfer effects because of the high availability of solvent water, which was assumed to be the proton source for HER (**Figure S3, S6**). We also observed that the CO partial current density was positively sensitive to $i_{0,CO}$ and α_{CO}, but more interestingly, negatively sensitive to the HER kinetics (i_{0,H_2} and α_{H_2}) (**Figures S2, S4**). As the HER current increases, the pH rises due to concomitant generation of OH⁻, and the generated OH⁻ anions consume reactant CO_2 via homogeneous buffer reactions thereby reducing the COER partial current.

Continuum simulations were then used to assess the accuracy of the traditional Tafel analysis **(**see **Section S7.1** of the **SI)** for simulated polarization curves where mass transport or competitive reactions were relevant. **Figure 5a-b** depict the results of performing traditional Tafel

analysis to extract the kinetic parameters from CO polarization curves generated by the simulation, all of which possess a constant CO Tafel slope but different values of L_{BL} (**Figure 5a**), or i_{0,H_2}(**Figure 5b**). As can easily be seen, even though the CO Tafel slope should be identical for all plotted polarization curves, the apparent Tafel slope as measured by a traditional approach is different for every curve, revealing the extent to which mass transport affects the apparent Tafel slope. Therefore, the continuum model is necessary to deconvolute the effects of mass transport from the intrinsic kinetics of the surface reactions.
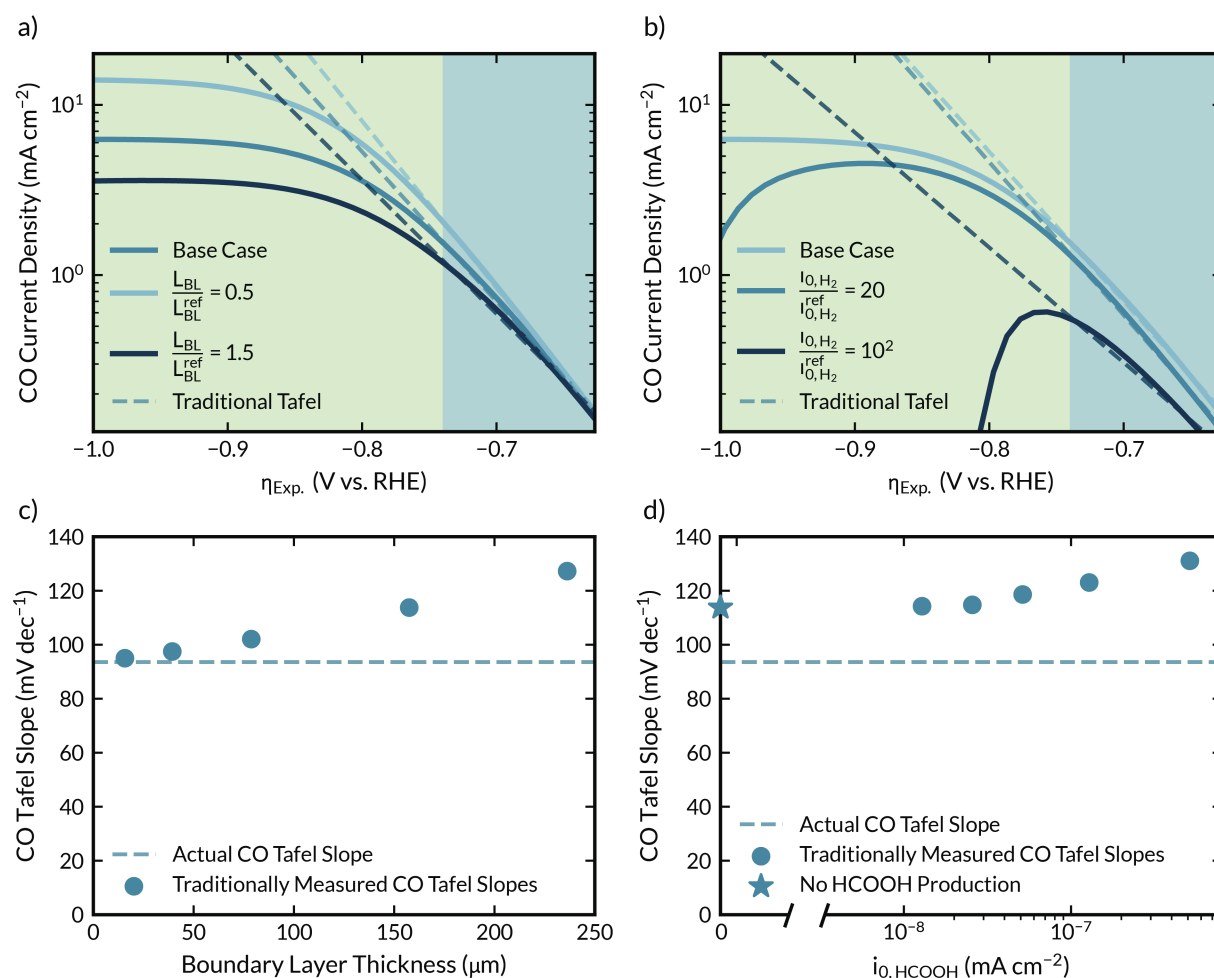

Figure 5: Analysis of traditional Tafel analysis accuracy under varying mass-transport regimes with a constant CO Tafel slope (**Table S4**). Effect of **(a)** L_{BL} and **(b)** i_{0,H_2} on CO Tafel analysis. Solid lines represent simulations where all parameters are fixed except for **(a)** L_{BL} or **(b)** i_{0,H_2}. In **(a)** and **(b)** dashed lines represent linear regression fits from traditional Tafel analysis (see **Section**

S7.1) (Tafel region in blue, and mass transport region in green). **(c)** Convergence of apparent Tafel slope to actual Tafel slope value as L_{BL} approaches zero. **(d)** Impact of competing HCOOH reaction on apparent Tafel slope. In **(c)** and **(d)** dashed lines represent the value of the Tafel slope as defined in the continuum model as representative of the intrinsic COER kinetics.

Intriguingly, when the apparent CO Tafel slope (**Figure 5b**) and $i_{0,CO}$ (**Figure S7**) are plotted against L_{BL}, they approach their intrinsic values as L_{BL} approaches zero. In other words, in the limit of no mass-transport losses of CO_2, traditional Tafel fitting is sufficient and accurate. This finding suggests traditional assessment of Tafel slopes could be done using data that are minimally affected by mass transfer. An attempt to do so has been reported recently by Jang *et al.*[37] A rotating cylinder electrode system was used to enhance mass transport to the cathode. However, the authors reported that mass transport could not be eliminated at moderate current densities for reactions with sparingly soluble reactants. Porous electrodes, which have boundary-layer thicknesses approaching the nanometer length scale, have also been suggested for determining the intrinsic kinetics of electrochemical reactions.[3,38] However, the chemistry and morphology of such electrodes were found to impact observed kinetics in non-trivial ways due to the potential of overlapping boundary layers, along with the complex multiphase (gas, liquid, and sometimes solid-electrolyte phases) transport occurring in the porous medium.[3] Therefore, continuum modeling of mass transport and the kinetics of bulk reaction occurring in an aqueous boundary layer (see below) will always be necessary for determination of Tafel parameters.

In addition to hydrodynamics, the presence of bulk reactions occurring in the thin boundary layer can impact the apparent Tafel slopes. **Figure 5b** and **S8** illustrate the effect of the HER current density on apparent CO kinetics, demonstrating that at high current densities for HER, the apparent CO kinetic parameters can be quite inaccurate. However, this competition for reactant CO_2 is indirect and is a result of consumption of HER-generated OH^- anions to form

HCO_3^- and CO_3^{2-} anions in the boundary layer, as opposed to direct electrochemical consumption. Indeed, many catalysts experience direct electrochemical competition for reactant CO_2. For instance, formic acid (HCOOH) forms competitively with CO on Cu, [6] Pd,[39] and Ag,[24] and such direct competition for CO_2 impacts the apparent Tafel slopes for these products. As shown in **Figure 5d** and discussed in greater detail in the **Section S7** of the **SI**, the occurrence of competing HCOOH formation dramatically increases the apparent CO Tafel slope beyond its intrinsic value. For the largest $i_{0,HCOOH}$ tested**,** corresponding to roughly equal co-generation of CO and HCOOH (**Figures S9-S10**), as has been observed on Cu[6] and Pd,[39] the CO Tafel slope is nearly 50 mV dec^{-1} larger than the reference value employed in the model (93.55 mV dec^{-1}). $i_{0,CO}, \alpha_{HCOOH}$, and $i_{0,HCOOH}$ exhibit similar inaccuracies (**Figures S12-S14**).

The transfer coefficient quantifies how much of the applied potential driving force goes to driving the rate of a given electrochemical reaction. In electrochemical synthesis systems, the applied potential driving force drives a suite of competitive surface reactions and overcomes losses attributable to low rates of mass transfer (*i.e.*, Nernstian losses). Thus, taking kinetic parameters directly from measured polarization data typically leads to an overestimation of the Tafel slope (and, hence, an underestimation of the transfer coefficient due to their inverse proportionality) by neglecting the potential losses associated with mass transport and competitive surface reactions. As mass transfer improves, and in the limit of a single surface reaction, the intrinsic kinetics can be measured experimentally. However, the presence of competing electrochemical reactions and poor mass transfer is the norm in electrochemical synthesis, rather than the exception. These results underscore the need for physiochemical models that enable determining the intrinsic Tafel parameters for individual reaction kinetics

unaffected by the effects of mass transport, bulk reactions occurring the mass-transfer boundary layer, or competing surface reactions.

4.2 Fitted Tafel Parameters

Having established that our model and approach for fitting Tafel parameters is capable of simultaneously fitting the parameters for CO and H_2 formation for different sets of data taken from the literature with quantified uncertainty (see **Section S11** of the **SI** for plots of all H_2 and CO polarization curves and the corresponding fitted Tafel parameter values), we sought to determine whether the fitted Tafel slopes and transfer coefficients converged to a set of cardinal values or to a set of values consistent with the transfer coefficients determined from DFT calculations. Bockris and co-workers derived what they refer to as cardinal values for the transfer coefficient of $\alpha_c = 0.5, 1.0, 1.5, etc.$[13] This can be done starting with **Equation S48** and assuming integer values for s and q, a v of 1, and a symmetry factor of the rate determining step, $\beta = 0.5$. Correspondingly, cardinal values for the Tafel slope (**Equation S82**) are 118, 59, 39, *etc.* Crucially, the symmetry factor, which is defined as the fraction of the applied overpotential that goes towards lowering the barrier of the cathodic reaction (as opposed to the anodic reaction),[40] will likely not be 0.5 for inner sphere electrochemical reactions such as CO_2R and HER on Ag, where some potential is lost in the double layer,[3] and the reaction intermediate is likely not equidistant in free energy from the reactants or products.[41] Nonetheless, many theoretical studies have employed the cardinal value of 0.5 for CO_2R.[10,42,43] It is also notable that the theoretical work of Singh *et al.* employs density functional theory (DFT) and finds an effective cathodic transfer coefficient of 0.49 and uses a microkinetic model to determine an exchange current density of

1.71×10^{-5} [mA cm^{-2}] for CO₂R to CO on Ag (110).[41] They also find transfer coefficients of 0.23 and 0.05 for the Volmer and Heyrovsky steps, respectively, where the latter is rate limiting.[41]
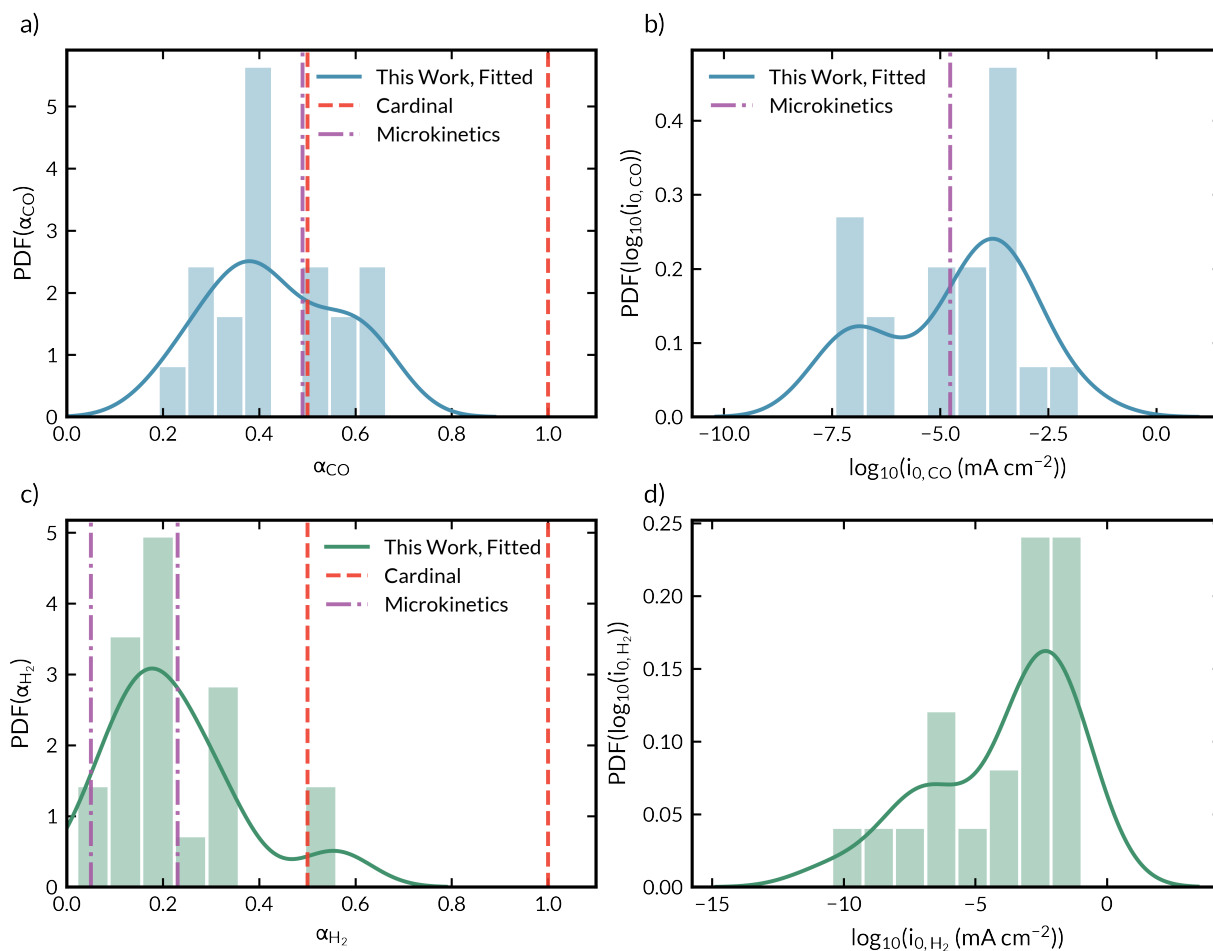

Figure 6: Probability distribution functions (PDF) (histogram) and kernel density estimates (KDEs) (solid lines) of the fit **(a)** α_{CO}, **(b)** $\log_{10}(i_{0,CO})$, **(c)** α_{H_2}, and **(d)** $\log_{10}(i_{0,H_2})$. The PDF depicts a histogram of the fitted parameters that has been scaled such that the integrated total of the bars adds to unity. The KDE represents a smoothed version of the PDF in which each bar is assigned a scaled basis function and these basis functions are superimposed to generate the smooth curve. Red dashed lines in both **(a)** and **(c)** correspond to cardinal values of the cathodic transfer coefficient as predicted by **Eq. S48**. It is important to note there are no cardinal values for the exchange current densities, as those are dependent on bulk electrolyte concentrations and surface roughness, which vary in each experiment, as well as rate constants for each kinetic step, which cannot be easily estimated. Purple dashed lines correspond to values expected from microkinetic modeling of Ag(110).[41] The transfer coefficients were determined via DFT and exchange current densities in the microkinetic work were obtained by fitting experimental partial current density

to the microkinetic model. Additionally, while the microkinetic work by Singh *et al.* provided values for α_{H_2} for both the Volmer and Heyrovsky steps, the work did not fit experimental HER partial current density and thus did not report an i_{0,H_2}.

Figure 6 illustrates the probability distribution functions (PDFs) and kernel density estimates (KDEs) for **(a)** α_{CO}, **(b)** $\log_{10}(i_{0,CO})$, **(c)** α_{H_2}, and **(d)** $\log_{10}(i_{0,H_2})$. These plots show that these parameters do not converge to a single set of values, as further demonstrated by the cumulative distribution functions shown in **Figure S19**. The fitted parameter distributions for the Tafel slopes and boundary layer thicknesses are given in **Figures S20** and **S21**. It is important to note that all fitted parameters lie within a range of physically acceptable values, and possess a tighter range than those previously reported for continuum models.[3] Additionally, the most probable values of the kinetic parameters for both CO and H_2 (determined as the maxima of the KDEs (see **Table S13**)) lie relatively close to the values reported by Singh *et al.* that were obtained via DFT of CO_2R and HER on Ag (110) (difference of 0.11 for α_{CO}, difference of 0.05 for the Volmer step α_{H_2}).[41] Notably, though, for HER, both DFT and the analysis of the KDE suggest transfer coefficients far from cardinality (much less than 0.5). Furthermore, the maximum value of the KDE for α_{c,H_2} lies close to that predicted by Singh for the Volmer step; whereas the Heyrovsky step was proposed to be rate limiting in that work. This discrepancy may be due to additional proton sources for the HER other than water (such as HCO_3^- anions), and future work should aim to develop a better physical model for HER in order to deconvolute these effects.

Additionally, consistent with the analysis in **Section 4.1**, we demonstrate that accounting for mass transfer helps mitigate the overprediction of Tafel slopes, shifting the distribution towards lower values when mass transfer is explicitly handled (**Figure S22**). It is important to note, that the size of the data set could simply be too small to observe a sharp distribution in the

fit parameters due to small variabilities or errors in the experimental measurements. Collecting more data in similar conditions could potentially lead to the distribution better predicting theoretically expected values. Nonetheless, the broad distribution of parameters makes it impossible to prescribe a unique set of values that are descriptive of the CO_2R on all Ag catalysts and indicate that Tafel parameters need be fitted for each individual Ag catalyst.

To address the spread of values in the fitted parameters, we note that the transfer coefficient itself may be a function of the applied potential as predicted by Marcus theory,[17] because at negative potential, the transition state is more initial-state like ($\beta_{RDS} \sim 0$) and at positive potential the transition state is more final-state like ($\beta_{RDS} \sim 1$).[44] However, Marcus inversion is not expected to be significant over the relatively small potential ranges studied experimentally, and all of the studies used were performed with nearly identical potential ranges. Thus, Marcus theory is unlikely to explain the spread in fitted parameters, and it is more likely that the observed spread in values is due to differences in surface morphology among different samples of Ag cathodes. Differences in surface roughness could be expected to contribute to the spread fit exchange current densities, as the roughness factor is implicitly lumped into that parameter (**Equation S65**).[3] Additionally, the Ag catalysts employed are typically polycrystalline. Clark *et al.* have shown that different Ag facets on polycrystalline Ag possess different intrinsic activities for CO_2R (**Figure S23**).[23] Therefore, the spread in transfer coefficient (and thus Tafel slope) could reflect the changes in the distribution of surface facets for different catalysts. Difference in surface coverage by adsorbates and by poisons may also impact the observed kinetic parameters.[45]

4.3 Compensation Effects in Electrocatalytic CO₂R on Ag

An important question is whether the transfer coefficients, exchange current densities, and the boundary layer thickness (α_{c,H_2}, $\alpha_{c,CO}$, i_{0,H_2}, $i_{0,CO}$, and L_{BL}) are correlated with each other. We first sought to assess whether the bulk electrolyte concentration and the boundary-layer thickness are correlated with the fitted transfer coefficients and exchange current densities, which should be intrinsic to the catalyst. **Figure S24** confirms that the lack of correlation between these parameters for all the fitted data. We next explored the correlation between the fitted values of α_c and i_0 for each reaction. The parameters α_c and $\log_{10}(i_0)$ should exhibit a negative, linear correlation with the slope of the correlation line related to the reaction order of the reactant and product species and their activity in the bulk electrolyte because the expression for i_0 is referenced to the activities of species in the bulk electrolyte (**Section S14.2** of the **SI**). While a negative correlation is observed for both reactions (**Figure**), the slopes are much more negative than would be expected from the analysis given in **Section S14.2** of the **SI** Additionally, these data were carried out using different bulk electrolyte concentrations and Ag electrodes having different roughness factors. As can be seen in **Equation S83** both factors impact the exchange current density. These effects are not explicitly deconvoluted from the correlation observed in **Figure** (roughness factors are seldom reported), so one should not expect any correlation in the plotted data. Vetter performed traditional Tafel analysis on various HER catalysts and demonstrated that while α_{H_2} was somewhat consistent across all tested catalysts, the $\log_{10}(i_{0,H_2})$ varied across these catalysts varied by many orders of magnitude and were uncorrelated with α_{H_2}.[9,46] Therefore, the apparent correlation between the fit α_c and $\log_{10}(i_0)$ is unexplained.
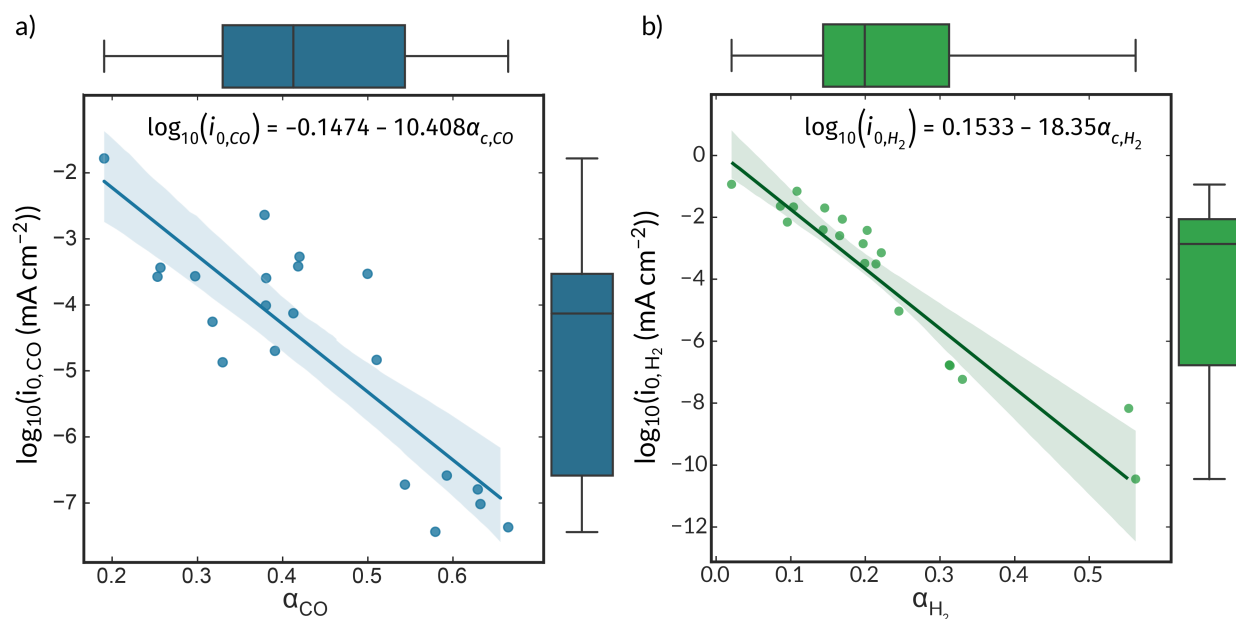
Figure 7: Compensation phenomena. Correlation plots for the fit cathodic transfer coefficients and the logarithm of the fit exchange current densities of **(a)** CO, and **(b)** H$_2$. The R^2 values for these fits are 0.73 and 0.90, respectively.

We note that a correlation has been observed in thermal catalysis between the pre-exponential factor and the activation energy, and is referred to as the "compensation effect".[47–51] Barrie has discussed the mathematical origins of this effect and its relationship to random experimental errors.[51] In this connection, Bond *et al.* have proposed a set of guidelines to establish when the effect is physically meaningful.[48] First, the dataset of must be sufficiently large; the range of transfer coefficients should be such that the largest value is at least 50% greater than the smallest. Second, the effects of the reaction order and bulk species concentration must be properly accounted for (**Figure S25-S26**). Lastly, we add that, for electrocatalysis, the effects of active surface area should be properly deconvoluted. For the data fit in this work, experiments were all reported based on geometric surface area of the cathode rather than the electrochemically active surface area (ECSA), making roughness effects difficult to deconvolute.

All considered, the existence of an apparent correlation likely suggests that, among other factors, the poor quality of experimental data in CO_2R leads to apparent compensation effects that contribute to the broad distribution of the fitted parameters observed in **Section 4.2**. Future work should use more sophisticated objective functions that weight data points according to their associated uncertainty, but the underlying issue is that many reports in CO_2R do not report polarization data with defined error bars. Additionally, reporting electrochemical data with respect to ECSA or using less-complex electrodes would also improve data quality for model fitting. Indeed, the poor quality of experimental data in electrocatalysis and the need for more easily interpretable electrocatalytic measurements has been well-documented in recent work.[52] The analysis presented here further underscores the need for better standards and protocols for acquisition of experimental data that can then be used to validate results obtained by theoreticians.

5. Conclusions

The present study describes a method for fitting Tafel parameters for multiple reactions occurring during the electrochemical reduction of CO_2 over Ag catalysts. This approach combines continuum modeling and advanced data-science methods (covariance matrix adaptation-evolutionary strategy (CMA-ES)) to fit the parameters appearing in the Tafel equations used to describe the kinetics of CO and H_2 formation. The method developed here avoids unquantifiable uncertainty associated with the subjective demarcation between the portions of the product polarization curves associated purely with reaction kinetics and that convoluted with the effects of mass transfer. A continuum model is employed to account for mass transport and bulk-phase

buffer reactions in these systems and reveals that the neglect of these phenomena leads to systematic overprediction of the Tafel slope and exchange current density obtained using traditional methods of analysis. The coupled CMA-ES continuum modeling approach is applied to 21 data sets for CO_2R on Ag obtained in similar electrochemical cells to determine rate parameters for CO_2R to CO and H_2 with quantified uncertainty. The fitted parameter distributions were analyzed to assess agreement of the rate parameters obtained with cardinal values and those predicted theoretically. A broad distribution of Tafel parameters across all data sets is observed, but the most probable values from the generated probability distributions lie reasonably close to values predicted from microkinetic analysis and DFT calculations. The distribution of values of the transfer coefficient and the exchange current density are attributed to difference in the structure and morphology of different Ag catalysts and to the quality of the data acquired for each catalyst. While a rough correlation between these two parameters is observed, we conclude that it is unphysical and more likely due to the poor quality of the experimental CO_2R data. This suggests that more rigorous standards need to be imposed on the collection of rate data. The product-specific transfer coefficient and exchange current density determined from such data could then serve as more stringent standards against which theoretical estimates of the Tafel parameters can be evaluated. Lastly, we note that our method of data analysis can easily be adapted to handle more complex reaction systems and in particular ones where both species mass transfer and bulk reactions influence the observed rates of product formation.

6.   Acknowledgements

7.   Author Contributions

JCB developed the model physics and COMSOL continuum model of CO_2 reduction on Ag used in the study. KRMC and AML developed the utilized covariance matrix adaptation MATLAB code applied to fit kinetic parameters. KRMC linked the COMSOL and MATLAB codes to fit kinetic and transport parameters in the continuum model. JCB and LMP developed the sensitivity analysis for the CO_2 reduction model. KM, AZW, and ATB provided guidance and direction for the project. KRMC and JCB prepared the original draft of the manuscript. All authors engaged in reviewing and editing the manuscript.

8.   References

1.   Blanco, D.E., and Modestino, M.A. (2019). Organic Electrosynthesis for Sustainable Chemical Manufacturing. Trends Chem. *1*, 8–10.

2.   De Luna, P., Hahn, C., Higgins, D., Jaffer, S.A., Jaramillo, T.F., and Sargent, E.H. (2019). What Would It Take for Renewably Powered Electrosynthesis to Displace Petrochemical Processes? Science (80-.). *364*.

3. Bui, J.C., Lees, E.W., Pant, L.M., Zenyuk, I. V., Bell, A.T., and Weber, A.Z. (2022). Continuum modeling of porous electrodes for electrochemical synthesis. Chem. Rev. *122*, 11022–11084.

4. Levi, P., Vass, T., Mandova, H., and Gouy, A. (2018). Chemicals — Analysis (International Energy Agency).

5. Goldman, M., Lees, E.W., Prieto, P.L., Mowbray, B.A.W., Weekes, D.M., Reyes, A., Li, T., Salvatore, D.A., Smith, W.A., and Berlinguette, C.P. (2021). Electrochemical Reactors. In Carbon Dioxide Electrochemistry: Homogeneous and Heterogeneous Catalysis (The Royal Society of Chemistry), pp. 408–432.

6. Nitopi, S., Bertheussen, E., Scott, S.B., Liu, X., Engstfeld, A.K., Horch, S., Seger, B., Stephens, I.E.L., Chan, K., Hahn, C., et al. (2019). Progress and Perspectives of Electrochemical CO_2 Reduction on Copper in Aqueous Electrolyte. Chem. Rev. *119*, 7610–7672.

7. Bui, J.C., Kim, C., King, A.J., Romiluyi, O., Kusoglu, A., Weber, A.Z., and Bell, A.T. (2022). Engineering Catalyst–Electrolyte Microenvironments to Optimize the Activity and Selectivity for the Electrochemical Reduction of CO_2 on Cu and Ag . Acc. Chem. Res.

8. Garg, S., Li, M., Weber, A.Z., Ge, L., Li, L., Rudolph, V., Wang, G., and Rufford, T.E. (2020). Advances and challenges in electrochemical CO_2 reduction processes: An engineering and design perspective looking beyond new catalyst materials. J. Mater. Chem. A *8*, 1511–1544.

9. Newman, J., and Thomas-Alyea, K.E. (2004). Electrochemical Systems 3rd ed. (John Wiley and Sons, Inc.).

10. Limaye, A., Zeng, J.S., Willard, A., and Manthiram, K. (2020). Bayesian Data Analysis Reveals No Preference for Cardinal Tafel Slopes in CO_2 Reduction Electrocatalysis.

11. Shinagawa, T., Garcia-Esparza, A.T., and Takanabe, K. (2015). Insight on Tafel slopes from a microkinetic analysis of aqueous electrocatalysis for energy conversion. Sci. Rep. *5*, 1–21.

12. Dunwell, M., Luc, W., Yan, Y., Jiao, F., and Xu, B. (2018). Understanding Surface-Mediated Electrochemical Reactions: CO_2 Reduction and beyond. ACS Catal. *8*, 8121–8129.

13. Bockris, J.O., and Nagy, Z. (1973). Symmetry Factor and Transfer Coefficient: A Source of Confusion in Electrode Kinetics. J. Chem. Ed. *50*, 839–843.

14. Weng, L.C., Bell, A.T., and Weber, A.Z. (2018). Modeling gas-diffusion electrodes for CO_2 reduction. Phys. Chem. Chem. Phys. *20*, 16973–16984.

15. Clark, E.L., Resasco, J., Landers, A., Lin, J., Chung, L.T., Walton, A., Hahn, C., Jaramillo, T.F., and Bell, A.T. (2018). Standards and Protocols for Data Acquisition and Reporting for Studies of the Electrochemical Reduction of Carbon Dioxide. ACS Catal. *8*, 6560–6570.

16. Agbo, P., and Danilovic, N. (2019). An Algorithm for the Extraction of Tafel Slopes. J. Phys. Chem. C *123*, 30252–30264.

17. Khadke, P., Tichter, T., Boettcher, T., Muench, F., Ensinger, W., and Roth, C. (2021). A simple and effective method for the accurate extraction of kinetic parameters using differential Tafel plots. Sci. Rep. *11*, 8974.

18. Rabinowitz, J.A., and Kanan, M.W. (2020). The future of low-temperature carbon dioxide electrolysis depends on solving one basic problem. Nat. Commun., 10–12.

19. Zhang, Z., Melo, L., Jansonius, R.P., Habibzadeh, F., Grant, E.R., and Berlinguette, C.P. (2020). pH Matters When Reducing CO_2 in an Electrochemical Flow Cell. ACS Energy Lett. *5*, 3101–3107.

20. Liu, X., Schlexer, P., Xiao, J., Ji, Y., Wang, L., Sandberg, R.B., Tang, M., Brown, K.S., Peng, H., Ringe, S., et al. (2019). pH effects on the electrochemical reduction of $CO_{(2)}$ towards C2 products on stepped copper. Nat Commun *10*, 32.

21. Hashiba, H., Weng, L.C., Chen, Y., Sato, H.K., Yotsuhashi, S., Xiang, C., and Weber, A.Z. (2018). Effects of electrolyte buffer capacity on surface reactant species and the reaction rate of CO2 in Electrochemical CO_2 reduction. J. Phys. Chem. C *122*, 3719–3726.

22. Yang, K., Kas, R., and Smith, W.A. (2019). In Situ Infrared Spectroscopy Reveals Persistent Alkalinity near Electrode Surfaces during CO_2 Electroreduction. J. Am. Chem. Soc. *141*.

23. Clark, E.L., Ringe, S., Tang, M., Walton, A., Hahn, C., Jaramillo, T.F., Chan, K., and Bell, A.T. (2019). Influence of Atomic Surface Structure on the Activity of Ag for the Electrochemical Reduction of CO_2 to CO. ACS Catal. *9*, 4006–4014.

24. Thevenon, A., Rosas-Hernández, A., Fontani Herreros, A.M., Agapie, T., and Peters, J.C. (2021). Dramatic HER Suppression on Ag Electrodes via Molecular Films for Highly Selective CO_2 to CO Reduction. ACS Catal. *11*, 4530–4537.

25. Li, H., Wen, P., Itanze, D.S., Hood, Z.D., Ma, X., Kim, M., Adhikari, S., Lu, C., Dun, C., Chi, M., et al. (2019). Colloidal silver diphosphide (AgP2) nanocrystals as low overpotential catalysts for CO_2 reduction to tunable syngas. Nat. Commun. *10*.

26.   Ma, M., Trześniewski, B.J., Xie, J., and Smith, W.A. (2016). Selective and Efficient Reduction of Carbon Dioxide to Carbon Monoxide on Oxide-Derived Nanostructured Silver Electrocatalysts. Angew. Chemie - Int. Ed. *55*, 9748–9752.

27.   Peng, X., Karakalos, S.G., and Mustain, W.E. (2018). Preferentially Oriented Ag Nanocrystals with Extremely High Activity and Faradaic Efficiency for CO_2 Electrochemical Reduction to CO. ACS Appl. Mater. Interfaces *10*, 1734–1742.

28.   Ma, M., Liu, K., Shen, J., Kas, R., and Smith, W.A. (2018). In Situ Fabrication and Reactivation of Highly Selective and Stable Ag Catalysts for Electrochemical CO_2 Conversion. ACS Energy Lett. *3*, 1301–1306.

29.   Koshy, D.M., Akhade, S.A., Shugar, A., Abiose, K., Shi, J., Liang, S., Oakdale, J.S., Weitzner, S.E., Varley, J.B., Duoss, E.B., et al. (2021). Chemical Modifications of Ag Catalyst Surfaces with Imidazolium Ionomers Modulate H2Evolution Rates during Electrochemical CO_2 Reduction. J. Am. Chem. Soc. *143*, 14712–14725.

30.   Hatsukade, T., Kuhl, K.P., Cave, E.R., Abram, D.N., and Jaramillo, T.F. (2014). Insights into the electrocatalytic reduction of CO_2 on metallic silver surfaces. Phys. Chem. Chem. Phys. *16*, 13814–13819.

31.   Kim, C., Jeon, H.S., Eom, T., Jee, M.S., Kim, H., Friend, C.M., Min, B.K., and Hwang, Y.J. (2015). Achieving Selective and Efficient Electrocatalytic Activity for CO_2 Reduction Using Immobilized Silver Nanoparticles. J. Am. Chem. Soc. *137*, 13844–13850.

32.   Yuan, X., Wu, Y., Jiang, B., Wu, Z., Tao, Z., Lu, X., Liu, J., Qian, T., Lin, H., and Zhang, Q.

(2020). Interface Engineering of Silver-Based Heterostructures for CO_2 Reduction Reaction. ACS Appl. Mater. Interfaces *12*, 56642–56649.

33.   Nakamura, M., Sato, N., Hoshi, N., and Sakata, O. (2011). Outer Helmholtz Plane of the Electrical Double Layer Formed at the Solid Electrode–Liquid Interface. ChemPhysChem *12*, 1430–1434.

34.   Bui, J.C., Kim, C., Weber, A.Z., and Bell, A.T. (2021). Dynamic Boundary Layer Simulation of Pulsed CO_2 Electrolysis on a Copper Catalyst. ACS Energy Lett. *6*, 1181–1188.

35.   Delacourt, C., and Newman, J. (2010). Mathematical Modeling of CO_2 Reduction to CO in Aqueous Electrolytes II. Study of an Electrolysis Cell Making Syngas (CO + H_2) from CO_2 and H_2O Reduction at Room Temperature. J. Electrochem. Soc. *157*, B1911–B1926.

36.   Akimoto, Y., Auger, A., Hansen, N., Auger, A., Hansen, N., Auger, A., Hansen, N., Auger, A., and Hansen, N. (2015). Tutorial : Evolution Strategies and CMA-ES (Covariance Matrix Adaptation) Continuous Domain Search / Optimization Continuous Domain Search / Optimization Objective Function Properties Goal. Proc. 2015 Annu. Conf. Genet. Evol. Comput., 333–355.

37.   Jang, J., Rüscher, M., Winzely, M., and Morales-Guio, C.G. (2022). Gastight rotating cylinder electrode: Toward decoupling mass transport and intrinsic kinetics in electrocatalysis. AIChE J. *68*.

38.   Higgins, D., Hahn, C., Xiang, C., Jaramillo, T.F., and Weber, A.Z. (2019). Gas-Diffusion Electrodes for Carbon Dioxide Reduction: A New Paradigm. ACS Energy Lett. *4*, 317–324.

39.   Nguyen, D.L.T., Nguyen, T.M., Lee, S.Y., Kim, J., Kim, S.Y., Le, Q. Van, Varma, R.S., and Hwang, Y.J. (2022). Electrochemical conversion of CO_2 to value-added chemicals over bimetallic Pd-based nanostructures: Recent progress and emerging trends. Environ. Res. *211*, 113116.

40.   Bard, A.J., and Faulkner, L.R. (2001). Electrochemical Methods: Fundamentals and Applications 2nd ed. (Wiley).

41.   Singh, M.R., Goodpaster, J.D., Weber, A.Z., Head-Gordon, M., and Bell, A.T. (2017). Mechanistic insights into electrochemical reduction of CO_2 over Ag using density functional theory and transport models. Proc. Natl. Acad. Sci. U. S. A. *114*, E8812–E8821.

42.   Hansen, H.A., Varley, J.B., Peterson, A.A., and Nørskov, J.K. (2013). Understanding trends in the electrocatalytic activity of metals and enzymes for CO_2 reduction to CO. J. Phys. Chem. Lett. *4*, 388–392.

43.   Liu, X.Y., Schlexer, P., Xiao, J.P., Ji, Y.F., Wang, L., Sandberg, R.B., Tang, M., Brown, K.S., Peng, H.J., Ringe, S., et al. (2019). pH effects on the electrochemical reduction of $CO_{(2)}$ towards C-2 products on stepped copper. Nat. Commun. *10*.

44.   Li, J., Stenlid, J.H., Ludwig, T., Lamoureux, P.S., and Abild-Pedersen, F. (2021). Modeling Potential-Dependent Electrochemical Activation Barriers: Revisiting the Alkaline Hydrogen Evolution Reaction. J. Am. Chem. Soc. *143*, 19341–19355.

45.   Motagamwala, A.H., and Dumesic, J.A. (2020). Microkinetic Modeling: A Tool for Rational Catalyst Design. Chem. Rev.

46.   Vetter, K.J. (1961). Elektrochemische Kinetik (Springer).

47.   Resasco, J., Abild-Pedersen, F., Hahn, C., Bao, Z., Koper, M.T.M., and Jaramillo, T.F. (2022). Enhancing the connection between computation and experiments in electrocatalysis. Nat. Catal. *5*, 374–381.

48.   Bond, G.C., Keane, M.A., Kral, H., and Lercher, J.A. (2000). Compensation Phenomena in Heterogeneous Catalysis: General Principles and a Possible Explanation. Catal. Rev. - Sci. Eng. *42*, 323–383.

49.   Bligaard, T., Honkala, K., Logadottir, A., Nørskov, J.K., Dahl, S., and Jacobsen, C.J.H. (2003). On the compensation effect in heterogeneous catalysis. J. Phys. Chem. B *107*, 9325–9331.

50.   Roduner, E. (2014). Understanding catalysis. Chem. Soc. Rev. *43*, 8226–8239.

51.   Barrie, P.J. (2012). The mathematical origins of the kinetic compensation effect: 1. the effect of random experimental errors. Phys. Chem. Chem. Phys. *14*, 318–326.

52.   Akbashev, A.R. (2022). Electrocatalysis Goes Nuts. ACS Catal. *12*, 4296–4301.